First comprehensive stable isotope dataset of diverse water units in a permafrost-dominated catchment on the Qinghai–Tibet Plateau

Yuzhong Yang[1, 2], Qingbai Wu[1, 2], Xiaoyan Guo[3], Lu Zhou[1], Helin Yao[1], Dandan Zhang[4], Zhongqiong Zhang[1, 2], Ji Chen[1, 2], Guojun Liu[1, 2]

[1] State Key Laboratory of Frozen Soil Engineering, Northwest Institute of Eco-Environment and Resources, Chinese Academy of Sciences, Lanzhou, China

[2] Qinghai-Beiluhe Plateau Frozen Soil Engineering Safety National Observation and Research Station, China

[3] Key Laboratory of Ecohydrology of Inland River Basin, Northwest Institute of Eco-Environment and Resources, Chinese Academy of Sciences, Lanzhou, China

[4] College of Energy and Power Engineering, Lanzhou University of technology, Lanzhou, China

Correspondence to: Yuzhong Yang (yangyuzhong08@lzb.ac.cn)

Definition or description of permafrost associated terms

Thermokarst lake: A lake occupying a closed depression formed by settlement of the ground following thawing of ice-rich permafrost or the melting of massive ice.

Ground ice: A general term referring to all types of ice contained in freezing and frozen ground

Pore ice: It termed interstitial or 'cement' ice, is the bonding material that holds soil grains together.

Segregated ice: It is formed by the migration of pore water to the 'frozen fringe' where it forms discrete lenses or layers.

Excess ice: defined as volume of ice in the ground that exceeds the total pore volume that the ground would have under natural unfrozen conditions.

Active layer: It is usually identified as a ground or rock above the permafrost table which undergoes seasonal freezing in winter.

Abstract

Considered as the Asian water tower, the Qinghai–Tibet Plateau (QTP) processes substantial permafrost, where its hydrological environments are spatially differed and can be easily disturbed by changing permafrost and melting ground ice. Permafrost degradation compels melting permafrost to become an important source of surface runoff, changes the storage of groundwater, and greatly influences the hydrological processes in permafrost regions. However, the evidences linking permafrost degradation and hydrological processes on the QTP are lacking, which increase the uncertainties of the evaluation results of changing permafrost on the water resources. Stable isotopes offer valuable information on the connections between changing permafrost (ground ice) and water components. It is therefore particularly important to observe the changes in the stable isotopes of different waterbodies, which can vary over hourly to annual timescales and truly capture the thawing signals and reflect the influence of permafrost (ground ice) on the regional hydrological processes. The Beiluhe Basin (BLH) in the hinterland of QTP were selected, which well integrates all the water components related to hydrological cycles, and is an ideal site to study hydrological effect of permafrost change. This paper presents the temporal data of stable isotopes ($\delta^{18}O$, δD, and d-excess) in different water bodies (precipitation, stream water, thermokarst lake, and groundwater) in the BLH produced between 2017 and 2022. In special, the first detailed stable isotope data of ground ice at 17 boreholes and 2 thaw slumps are presented. A detailed description of the sampling processes, sample pretreating processes, and isotopic data quality control is given. The data firstly described the full seasonal isotope amplitude in the precipitation, stream, and thermokarst lakes, and delineated the depth isotopic variability in ground ice. Totally, 554 precipitation samples, 2402 lakes/ponds samples, 675 stream water samples, 102 supra-permafrost water samples, and 19 sub-permafrost water samples were collected during six years' continuous sampling work. Importantly, 359 ground ice samples at different depths from 17 boreholes and 2 profiles were collected. This first data set provides a new basis for understanding the hydrological effects of permafrost degradation on the QTP. It also provides supports on the cryospheric study on the Northern Hemisphere.

1 Introduction

Recognized as the main components of cryosphere, permafrost plays critical roles in climate change, evolution of ecosystem, water cycle, and human activities (Brown et al., 1997). Throughout the past several decades, the thermal stability of permafrost has suffered serious threats (Cheng et al., 2019; Douglas et al., 2021; Biskaborn et al., 2019) caused by continuous global warming (IPCC, 2019). Latest IPCC report indicates that up to 24-69% of permafrost will disappear by 2100 (IPCC, 2019). Warming and thawing of permafrost and an overall reduction in the ice content have been predicted under future climate change scenarios (IPCC, 2019). Dramatic permafrost degradation and ground ice melting has changed the regional hydrological processes (Yang et al., 2011; Quinton and Baltzer, 2013; Rogger et al., 2017), enhanced the hydraulic connections (Connon et al., 2014; Cheng and Jin, 2013; Zhang et al., 2013), and compel ground ice to become an important source of surface runoff and lakes (Yang et al., 2019; Zhang et al., 2005; Lawrence and Slater, 2005). Accordingly, clarifying the influence of degrading permafrost on the ecohydrology and water resources is of great significance to the protection of eco-environment and effective utilization of fresh water in permafrost regions in the world.

The Qinghai–Tibet Plateau (QTP) is known as the "Asia Water Tower", which is considered as the headwater regions of many large rivers in Asia (Immerzeel et al., 2010). As the world's largest high-altitude permafrost regions (Cheng et al., 2019), the QTP contains as many as 1.06×10^6 km^2 of permafrost and 12700 km^3 of ground ice (Cheng et al., 2019). Extensive development of permafrost and substantial reserves of ground ice has exerted critical roles in climate change, ecosystem transition, water resource, carbon budget, and infrastructure of QTP (Zhao et al., 2020; Liu et al., 2022a; 2022b). Accordingly, the QTP has been becoming a hot region for scientists from different research fields (Wang et al., 2006; Yang et al., 2019; Zhao et al., 2021). During recent decades, the QTP has been experiencing severe warming over the past 50 years (Yao et al., 2013; Ran et al., 2022; Kuang and Jiao, 2016), which leads to accelerated permafrost degradation (Wu and Zhang, 2010; Zhao et al., 2021), and thereafter greatly affected the plateau water-eco environment-carbon cycle systems (Wang et al., 2023a; Yi et al., 2014; Liu et al., 2022a).

So far, due to the harsh climate conditions, inconvenient transportations, and high experimental costs of site-specific field data, there has been a lack of comprehensive research on different water bodies in permafrost regions over a long time on the QTP, making it challenging to study the water cycle and hydrological processes associated with changing permafrost. In addition, traditional method (e.g., modelling, GRACE satellite technique) is thus difficult to delineate the processes of ice-water transition truly and comprehensively, greatly increasing the uncertainties of evaluation results about the impacts of permafrost degradation on the hydrological processes (Guo et al., 2017). Hydrogen and oxygen stable isotopes ($\delta^{18}O$, δD) are widely existing natural tracers, which are considered to be ideal tools to identify temporal-spatial patterns of precipitation-river-lake-groundwater systems (Knapp et al., 2019; Narancic et al., 2017; Vystavna et al., 2021) and therefore to delineate hydrological connectivity under degrading permafrost (Wang et al., 2022; Streletskiy et al., 2015; Yang et al., 2019). Furthermore, the stable isotopes can well document the signals of ice-water phase transition and freezing history, making them provide convenient means for investigating of ground ice evolution (Michel, 2011; Lacelle et al., 2013; Porter et al., 2019) in permafrost.

Accordingly, continued observations of the stable isotope data, required to understand the changes of hydrological processes and water vapor cycles linked with permafrost degradation and ground ice melt, are therefore of great importance. However, the acquisition of long time series stable isotopic data in permafrost-dominated catchment on the QTP is challenging, especially for the stable isotope records of thermokarst lakes/ponds and ground ice on the QTP, which are extremely scarce. It greatly limits the deep understanding of the hydrological processes under thawing permafrost.

In this paper, we provide information on the study site and full documentation of the water components in a typical permafrost watershed (Beiluhe Basin, BLH) on the QTP. The data sets presented here, including the stable isotopes of daily precipitation, monthly isotope data of surface waters (stream and thermokarst lakes/ponds) and groundwater, and ground ice within 20 m in depth, will be of great value for tracking water vapor cycles, for capturing the signals of permafrost thawing and delineating the hydrological routines of permafrost meltwater, and in continuing baseline studies for future permafrost degradation trend analysis and water resources evaluations on the QTP. Special emphasis is given to the critical role of BLH for research in the hinterland of QTP to diagnose the effect of thawing permafrost.

2 Study area

A typical permafrost catchment, namely the Beiluhe Basin (BLH; Fig. 1), was selected to comprehensively observe the hydrological processes under changing permafrost. The BLH is situated in the interior of the QTP, with elevations of 4,500 to 4,600 m.s.l. It is considered as a core region of the Hoh Xil Nature Reserve region and provides the best habitats for wild animals on the QTP. The BLH is also identified as one of the most fragile and sensitive ecosystems in the world due to the diversities in the ecosystems, which including swamp meadow, alpine meadow, degrading alpine meadow, alpine steppe, desert alpine grassland, sparse grassland (Yin et al., 2017). According to the meteorological station of BLH, between 2017 and 2022, the annual mean air temperature ranged between -3.57 °C (2019) and -2.43 °C (2022), the annual precipitation ranged between 394 mm (2020) and 556 mm (2018), the duration of negative air temperature exceeds 200 d.

The BLH is closely connected with the Source Area of Yangtze River (i.e., the Tuotuohe River), and is characterized by a complex hydrological system of streams (Yang et al., 2017), thermokarst lakes (Yang et al., 2016; Niu et al., 2011), groundwater (springs), as well as abundant ground ice (Yang et al., 2013; 2016). Thermokarst lakes are widely distributed in the basin, with a total lake-number of more than 1200 (Luo et al., 2015) which are showing gradual increase trend. In addition, controlled by the piedmont faults of Gushan Mountain (Fig. 1) in the BLH, the natural springs are extensively exposed on the ground, which are the main sources of small streams. The connectivity of lakes, streams, groundwater, as well as melting water from permafrost exerted important roles on how ecological and hydrological systems are propagated in this basin.

The BLH is located in the zone of continuous ice-rich permafrost in the Changtang Basin. The permafrost thickness is approximately 20–80 m thick. Mean annual ground temperature (MAGT) at 15 m depth ranges from -1.8 to -0.5°C and the active layer thickness is 1.6–3.4 m (Wu et al., 2015). Ground ice is abundant in this region, and as high as 70% of this area has a volumetric ice content (VIC) higher than 30% (Luo et al., 2015). Most of the ground ice in the BLH is identified as excess ice (Niu et al., 2002), which could melt out to recharge supra-permafrost water (springs) or even surface water (Yang et al., 2016). Accordingly, the BLH is a natural laboratory to conduct field hydrological observations, the observation data can facilitate the developments of human infrastructure and ecological restoration of QTP.

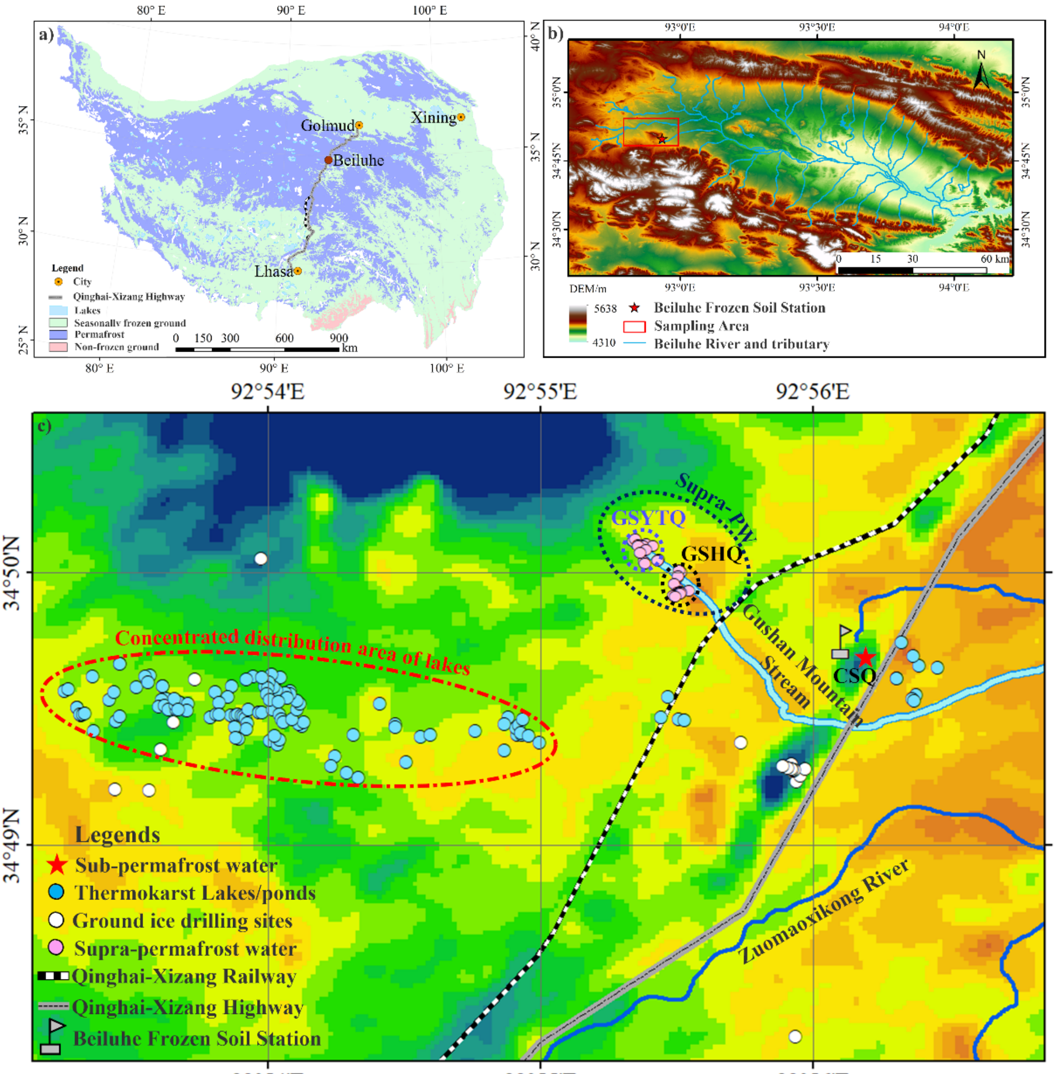

Figure 1: (a) Location of the Beiluhe Basin on the QTP, (b) Distribution of our study area in the Beiluhe Basin, and (c) the specific sampling sites of different water components in the BLH. Supra-PW denotes the Supra-permafrost water.

3 General design of the monitoring network

From 2017 to 2022, we set up sampling sites of precipitation, stream, thermokarst lake/pond, groundwater (including supra-permafrost water and sub-permafrost water), and ground ice in the BLH basin (Fig. 1). The precipitation stable isotope sampling site was setup at the BLH frozen soil station (Fig. 1). A rain gauge was installed to collect daily rain, and a steel plate was put on the roof to obtain as much as snow samples. In addition, we selected a typical small stream (defined as Gushan Mountain Stream, GMS) in the BLH Basin, which originates from four natural springs in foothill of the Gushan Mountain (Fig. 2; Fig. S1). This stream is 4.8 km in length. The vegetation along this stream is mainly composed of deserted steppe. A total of 25 fixed points along the stream were selected to collect water samples during the ice-free seasons between June and October. Furthermore, a typical thermokarst lake belt located in the southwestern of the BLH station on the QTP were selected to observe lake water balance (Fig. 1). For the groundwater observation, we selected two areas with substantial natural opening springs occurring, i.e., springs along the both sides of the observation stream (named as GSHQ) and spring in the source area of this stream (named as GSYTQ) (Fig.1; 2). Given the intermittent occurrence of these springs among different years and their unstable isotopic signals, we identified them as supra-permafrost water. In addition, a perennial spring (CSQ; Fig. 1) for domestic water supply behind the BLH station (Fig. 1), with its aquifer depth (reaching 92 m) being deeper than the permafrost thickness (~50m) in the BLH, is selected to conduct continuous sampling work. In regards to the small fluctuations in water level all the year and little interannual differences in stable isotopes of spring, we identified it as the observation site of sub-permafrost water. In order to detect the permafrost changes and clarify the characteristics of ground ice conditions, 17 boreholes (20 m in depth) were drilled in the BLH basin (Fig. 1). All visible ice samples were collected in the field.

Meanwhile, an auto meteorological station is set up in the center of the BLH since 2005. Air temperature is measured in a solar radiation shield at 2.0 m above the ground surface. The precipitation amount from nearby meteorological station was measured using a T200B rain/snow gauge (Geonor, Norway), and data were recorded every 30 min. The meteorological data have high quality and continuity with very limited missing data due to regular maintenance by Beiluhe Frozen soil station.

Table 1 Location information on the sampling sites in the Beiluhe Basin

Sampling sites	Precipitation	Stream	Thermokarst lakes/ponds	Springs	Ground ice
Latitude/°	N 34.83	N 34.82~34.84	N 34.82~34.83	N 34.83~34.84	N 34.82~34.83
Longitude/°	E 92.94	E 92.92~92.93	E 92.89~92.93	E 92.92~92.93	E 92.93~92.89
Altitude/m	4628	4668~4697	4704~4752	4752~4771	4629~4691

4. Sample collection and processing

4.1 Sampling and preservation

4.1.1 Precipitation sampling work

According to the International Atomic Energy Agency/Global Network of Isotopes in Precipitation (IAEA/GNIP) precipitation sampling guide, a precipitation collector was manually constructed in an open area near the BLH meteorological station. To avoid the contamination of water vapor from evaporation of shallow soil and surface water, and the mixing of windblown snow, this collector was installed 2 m above the ground. We define one complete precipitation day beginning at 20:00 on one day, and ending at 20:00 in the next day, then the one sample was collected. All the rainfall samples were immediately collected after the end of precipitation to minimize the effects of evaporation. Hail and snow samples were filled in pre-cleaned plastic bags, the plastic bags were exhausted and sealed to avoid the water vapor exchange, and all samples in sealed bags were melted room temperature (25 °C). In order to clarify the changes comprehensively and accurately in the precipitation isotopes in the BLH Basin, we tried to collect all samples during every precipitation event, including light rain and short-time events (usually with precipitation amount of less than 5 mm). Accordingly, a wide mouth stainless steel plate (400 mm×600 mm) was used to collect as much as samples of light rain and short-time rain/snow events for analysis.

Regarding preserving samples, 100 ml high-density polyethylene (HDPE) bottles were used. Before the sampling, the bottles were washed three times with rain water and then rapidly filled. Totally, 554 precipitation samples were collected, including 224 rain samples, 203 snow samples, 85 hail samples, and 42 sleet samples.

4.1.2 Stream, thermokarst lakes/ponds, and groundwater sampling

Samples of thermokarst lakes/ponds (Fig. 2) were collected by hand using a self-made water sample collector at monthly intervals during ice-free seasons (between May and October) from 2017 to 2022 in the BLH Basin (Fig. 1). During the observation periods, the occurrence numbers of thermokarst lakes dynamically changed among different sampling years (Table 2) due to the interannual variations in the precipitation, active layer thickness, supra-permafrost water, as well as near-surface ground ice. Partial of sampled lakes disappeared in the next sampling year and additional new lakes emerged. Accordingly, we obtained as many as lake water samples to constrain the seasonal changes in the lake water hydrology and try to clarify the influence of permafrost and climate on the water balance of thermokarst lakes in this region. Influenced by the Covid-19 and lockdown policies between August, 2022 to December, 2022 in China, only two months' sampling work (June and July) was conducted in 2022. Lake water samples were taken at the center of lakes from 20–40 cm below water surface. The running water samples of stream water samples were collected at each fixed point 20-30 cm beneath the water surface. In addition, the supra-permafrost water and sub-permafrost water were randomly collected using a man-made water ladle at the location where the springs gushing out during each field work. The water ladle was washed using the spring water before sampling.

Totally, as many as 2402 thermokarst lakes/ponds samples, 675 stream water samples (Table 2), 102 supra-permafrost water samples, and 19 sub-permafrost water samples were collected during six years' continuous sampling work.

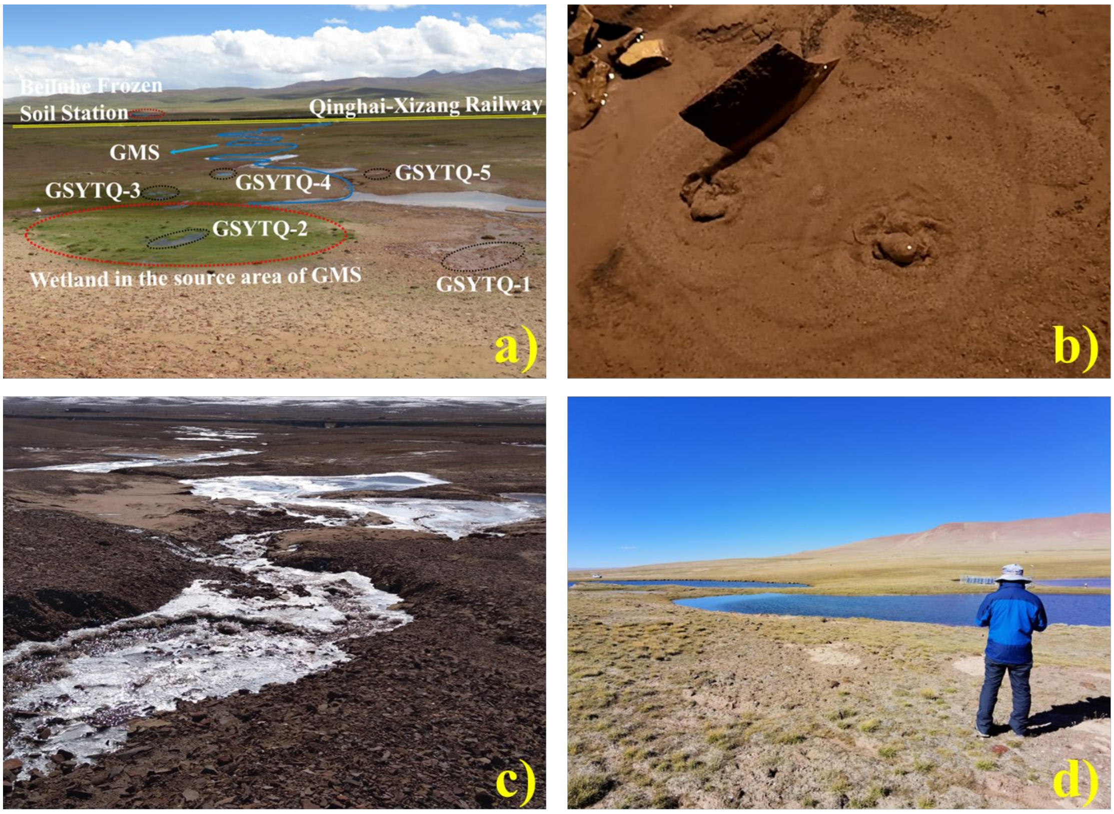

Figure 2: (a) General conditions of Gushan Mountain Stream (GMS) and distribution of springs; (b) Typical feature of one spring gushing outs from sand sediment; (c) Overview picture of GMS; and (d) Sampling thermokarst lakes in the BLH.

Table 2 Sampling descriptions of surface water in the BLH

Sampling Information		**Number of samples**	
		Thermokarst lake/pond	**Stream**
Sampling date	Jun-17	23	25
	Jul-17	76	25
	Aug-17	74	25
	Sep-17	99	25
	Oct-17	72	25
	May-18	74	N.A
	Jun-18	14	25
	Jul-18	45	25
	Aug-18	110	25
	Sep-18	93	25
	Oct-18	106	25
	May-19	80	N.A
	Jun-19	115	25
	Jul-19	134	25
	Aug-19	87	25
	Sep-19	85	25
	Oct-19	110	25
	Jun-20	86	25
	Jul-20	124	25
	Aug-20	116	25
	Sep-20	93	25
	May-21	73	25
	Jun-21	70	25
	Jul-21	100	25
	Aug -21	100	25
	Sep-21	94	25
	Jun-22	75	25
	Jul-22	74	25
Total sample size		2402	675

4.1.3 Ground ice sampling

To clarify the characteristics of ground ice and its role on the local hydrological cycles and regional eco-environment, we have designed 17 boreholes (~20 m in depth) in the BLH basin (Fig. 1). A total of 12 boreholes were drilled near the Qinghai-Tibet Highway (QTH) in 2014, and 5 boreholes were distributed in the center of BLH basin, which were drilled between 2011 and 2021. In addition, 2 thaw slumps were dug (Fig. 1). Frozen soil cores were extracted from different depths using a mechanical drilling rig with a drilling diameter of 157 mm (Fig. 3). All visible ground ice samples were collected immediately after the core barrel was pulled out. During sampling work, the disposable PE gloves were used, and the exterior of each sample was removed to avoid contamination from mud and the surplus water in the borehole. Totally, 355 ground ice samples were collected from 17 boreholes and 4 samples were obtained from 2 profiles (Fig. 3; Table 3).

Figure 3: Field permafrost drilling work and various types of ground ice obtained during drilling.

Table 3 Borehole drilling and ground ice sampling information in the BLH

Borehole name	Drilling time	Depth range of ice sampling/m	Ground ice types	Sample number
BLH-L-1	Aug-2014	4.8-14.9	Pore ice/segregated ice/excess ice	10
BLH-L-2	Aug-2014	2.7-14.3	Pore ice/segregated ice/ excess ice	28
BLH-L-3	Aug-2014	2.9-14.8	Pore ice/segregated ice/ excess ice	20
BLH-L-4	Aug-2014	2.55-14.2	Pore ice/segregated ice/ excess ice	34
BLH-L-5	Aug-2014	2.3-14.0	Pore ice/segregated ice/ excess ice	15
BLH-L-6	Aug-2014	2.6-14.3	Pore ice/segregated ice/ excess ice	11
BLH-R-1	Aug-2014	3.0-12.9	Pore ice/segregated ice/ excess ice	10
BLH-R-2	Aug-2014	1.9-14.9	Pore ice/segregated ice/ excess ice	20
BLH-R-3	Aug-2014	1.25-8.1	Pore ice/segregated ice/ excess ice	17
BLH-R-4	Aug-2014	1.8-11.9	Pore ice/segregated ice/ excess ice	32
BLH-R-5	Aug-2014	1.7-13.8	Pore ice/segregated ice/ excess ice	36
BLH-R-6	Aug-2014	2.1-14.6	Pore ice/segregated ice/ excess ice	22
DZK	Aug-2012	0.0-20.55	Pore ice/segregated ice/ excess ice	27
ZK-1	Aug-2011	12.4-17.4	Pore ice/segregated ice/ Pure ice layer	28
ZK-2	Aug-2011	3.0-7.2	Pore ice/segregated ice/ excess ice	15
ZK-3	Aug-2011	2.6-12.8	Pore ice/segregated ice/ excess ice	13
ZK-4	Aug-2011	2.2-5.5	Pore ice/segregated ice/ excess ice	17
Z	Oct-2021	2.0-3.0	Thaw slump ice	2
FBX	Oct-2021	2.0-3.0	Thaw slump ice	2

4.1.4 Sample storage

Liquid water storage: All the samples were transferred to 100 ml high-density polyethylene (HDPE) bottles. The sample bottles were filled up without bubbles and sealed with parafilm. The collection date sample types (precipitation, lake water, stream water, groundwater) were labelled. For the precipitation samples, the precipitation types (rain, snow, hail) were recorded. All the samples were stored at 4°C and shipped to the State Key Laboratory of Frozen Soil Engineering (SKLFSE) in Northwest Institute of Eco-Environment and Resources, Chinese Academy of Sciences (CAS), China.

Ground ice storage: All the treated raw frozen soil samples were immediately preserved in HDPE bottles. The massive ice and pure ice layers were sealed in the pre-cleaned plastic bags. The depths and drilling site information were recorded. All the frozen soil and ground ice samples were kept frozen at −4°C in the field to avoid sublimation of the ice and evaporation of the water in the soil.

4.2 Sample pretreatment and stable isotope analysis

Before analyzing, each liquid sample was pretreated to remove the impurities through 0.22-μm disposable membrane filters. The frozen soil samples and pure ground ice samples were allowed to completely melt at 4 °C in sealed plastic bags. The supernatant water from thawed soil and meltwater from ground ice were also filtered through a 0.22-μm membrane. The processed liquid water samples were filled in 2 ml analytical vial and were stored in a cold room (4 °C) in the dark for the stable isotopes ($\delta^{18}O$ and δD) analysis within 1 week.

The $\delta^{18}O$ and δD ratios were measured at SKLFSE, using an Isotopic Liquid Water and Water Vapor Analyzer (Picarro L2130-i, U.S.) based on the wavelength-scanned cavity ring down spectroscopy technique. The guaranteed instrument precision was 0.025 ‰ for the $\delta^{18}O$ value measurements and 0.1 ‰ for the δD value measurements. The isotopic values were reported using notation representing the per mille (‰) relative difference with respect to the IAEA Vienna Standard Ocean Water (VSMOW) standard following Eq. (1):

$$\delta=(Rsa/Rst -1) \times 1000 ‰$$

4.3 Quality control of data

4.3.1 Sampling errors

The precipitation samples were transferred to HDPE bottles immediately. If multiple rain/snow events occurred during one sampling day, the water sample from one single precipitation event was firstly collected. At the end of one complete sampling day, all the samples collected from single event were mixed. If the precipitation types changed during one sampling day, different samples were collected separately. The final complete samples were kept cool at 4 °C. All we have done is to avoid the influence of evaporation on enrichment of D and ^{18}O and ensure the originality of samples.

During the sampling work of thermokarst lakes/ponds and streams, we do our best to control the sampling time at the same period during every month (controlling the sampling time within one week, i.e., between 17th and 22th in every month) to make sure that all the samples can represent the average level of the whole month. The sampling HDPE bottles were precleaned three times using the raw water. Lake water was taken at the center of lakes from 20–40 cm beneath water. The running water samples of stream were collected at each fixed point 20-30 cm beneath the water surface.

4.3.2 Analytic errors

Before we started to analyze the samples, we firstly prepared 14 distilled or tap water samples with the same stable isotopes to test the stability of our analyzer. The precisions of the $\delta^{18}O$ and δD values were calculated by calculating the 1-sigma standard deviation of groups of 12 injections and then calculating the average of these standard deviations. In order to ensure the data quality, the "high precision" mode was employed during analysis. Under this mode, the analyzing time for each injection is about 8.75 minutes. The drift of the analyzer was determined by taking the mean of these same 12 groups of measurements and calculating the difference between the maximum and minimum means. All these measured precision and drift values were less than those of the guaranteed precision (0.025‰ and 0.1‰ for $\delta^{18}O$ and δD) and drift values (0.2‰ and 0.8‰ for $\delta^{18}O$ and δD), indicating that the analyzer achieve both a good repeatability and a good reproducibility. If the measured precision and drift values were not passed the guaranteed values, the comprehensive inspection of the analyzer was conducted, i.e., the instrument analyzing system, the vaporizer module, as well as the quality of dry nitrogen. After completing all checking processes, we repeated the analysis of 14 distilled/tap water samples and calculated the drift values until they passed the guaranteed values. The results were normalized to the V-SMOW-SLAP scale by analyzing internal standards before and after each set of ten samples. Five laboratory standards (provided by LICA United Technology Limited, Beijing, China) with given isotopic values were inserted before 10 samples, which were used for instrument calibration: with $\delta^{18}O$ values of −21.28‰, −16.71‰, −11.04‰, −7.81‰, and −2.99‰, and δD values of −165.7‰, −123.8‰, −79.6‰, −49.2‰, −9.9‰. The best-fit linear relationship between the five known calibration values and the analyzer's reported values was determined. The slope and intercept of the best-fit line through these points are used to calibrate the results of our samples.

To avoid memory effects, the first three results of measurements were discarded and arithmetic mean values were calculated from the last three injections. During the analyzing process, the real-time data of water concentration of all injections were controlled within a range between 19000 ppm and 20000 ppm and with a standard deviation of less than 200 ppm. Once the water concentration values appear to decrease, the work was stopped and the syringe was detached to wash using the deionized water. All measurements were post-processed with the Picarro ChemCorrect™ software to monitor the organic contamination and correct the data.

5 General characteristics of stable isotopes in different water components

5.1 Variations in the stable isotopes of different water components

5.1.1 Precipitation

The stable isotopes of precipitation exhibit a remarkable seasonal variability during six years' observations (Fig. 4). The $\delta^{18}O$ and δD of the local precipitation in the BLH Basin ranged from -30.4‰ to 6.2‰ and from -238.0‰ to 65.4‰, respectively. The d-excess ranged between -37.5‰ and 44.5‰. The amount-weighted average values of annual precipitation are -10.9‰, -72.1‰, and 15.4‰ for $\delta^{18}O$, δD, and d-excess, respectively. As shown, the $\delta^{18}O$ and δD display distinct seasonal patterns with high values in summer and low values in winter (Fig. 2; Fig. S2), it is due to the changes in moisture sources and the influence of local climate conditions (Guo et al., 2022; Tian et al., 2005; Guan et al., 2013; Bershaw et al., 2012).

5.1.2 Surface water bodies

For comparison, the $\delta^{18}O$ and δD of thermokarst lakes/ponds are more positive than those of precipitation due to strong evaporation and resultant enrichments of heavier isotopes in lake water (Yang et al., 2016; Narancic et al., 2017; Ala-aho et al., 2018). The $\delta^{18}O$ ranged from -14.4‰ to 5.7‰ (mean: -6.0‰), the δD is between -104.1‰ and 22.6‰ (mean: -48.0‰), and the d-excess is ranged from –35.8‰ to 21.8‰ (mean: -0.1‰), respectively. Similarly, the isotopic patterns of thermokarst lakes/ponds exhibited strong seasonal variations (Fig. 4; Fig. S3), which is due to the changes in source waters (i.e., precipitation, meltwater of thawing permafrost/ground ice, groundwater) and alternations of evaporation degrees due to air temperature fluctuations (Narancic et al., 2017; Yang et al., 2021; Aichner et al., 2022; Zhu et al., 2022). Generally, the heavy isotope contents of lakes/ponds are lower in August and September (Fig. 4; Fig. S3), which is attributed to the recharges of monsoonal precipitation and water with more negative isotopes fed by melting ground ice (Gibson et al., 2015; Yang et al., 2021). In comparison, majority of isotope values of lakes/ponds are positive in May, June, July, and October (Fig. 4; Fig. S3) due to evaporation and recharge of isotopic-enriched precipitation water.

For the streams, the isotope values varied from -13.7‰ to -7.2‰ ($\delta^{18}O$, mean: -11.1‰) and from -83.8‰ to -53.3‰ (δD, mean: -73.6‰), and the d-excess is ranged from -0.6‰ to 25.6‰ (mean: 15.0‰), respectively. The mean values are equivalent to the average values of annual precipitation in the BLH. Compared with thermokarst lakes/ponds, the $\delta^{18}O$ values of stream water exhibited relatively stable patterns (Fig. 4) due to short residence time (Yang et al., 2021; Wang et al., 2023b; Song et al., 2017), which indicates weak evaporation. However, the stream isotopes also represented seasonal variations during six year's observation (Fig. 4; Fig. S4), lower values were prevailing in August and September. The temporal changes of stream isotopes are mainly influenced by the seasonal variability of evaporation (Yang et al., 2017) and differences in the source water, i.e., alternative replenishment of precipitation, melting ground ice, and groundwater (Streletskiy et al., 2015; Yang et al., 2019; Ala-aho et al., 2018).

The two kinds of supra-permafrost water (i.e., GSHQ and GSYTQ) exhibited similar seasonal trend (Fig. 4). For comparison, the GSHQ displayed relatively more positive isotopic peaks during whole sampling periods (Fig. 4), with $\delta^{18}O$ ranging from -13.3‰ to -5.8‰ (mean: -11.2‰), the δD is ranging between -86.7‰ and -39.0‰ (mean: -74.2‰), and the d-excess varying from 6.5 to 22.4‰ (mean: 15.1‰), respectively. The isotopes of GSYTQ varied from -13.5‰ to -8.4‰ (mean: -11.4‰), the δD is ranging between -83.2‰ and -50.6‰ (mean: -73.8‰), and the d-excess is varying from 4.6 to 25.1‰ (mean: 16.9‰). The isotopic peaks of the two types of springs lagged behind those of precipitation (Fig. 4), indicating replenishments of precipitation via infiltration. By contrast, the stable isotopes of sub-permafrost water are more negative than those of supra-permafrost water, ranging between -12.7‰ and -11.1‰ (mean: -11.8‰) for $\delta^{18}O$, from -83.7‰ to -77.7‰ (mean: -80.7‰) for δD, and from 10.9‰ to 17.7‰ for d-excess (mean: 13.5‰). In addition, they kept nearly stable over long time series (Fig. 4), suggesting unchanged sources of isotopically light water (e.g., monsoonal precipitation, meltwater from thawing permafrost, et al) and insignificant influence by precipitation.

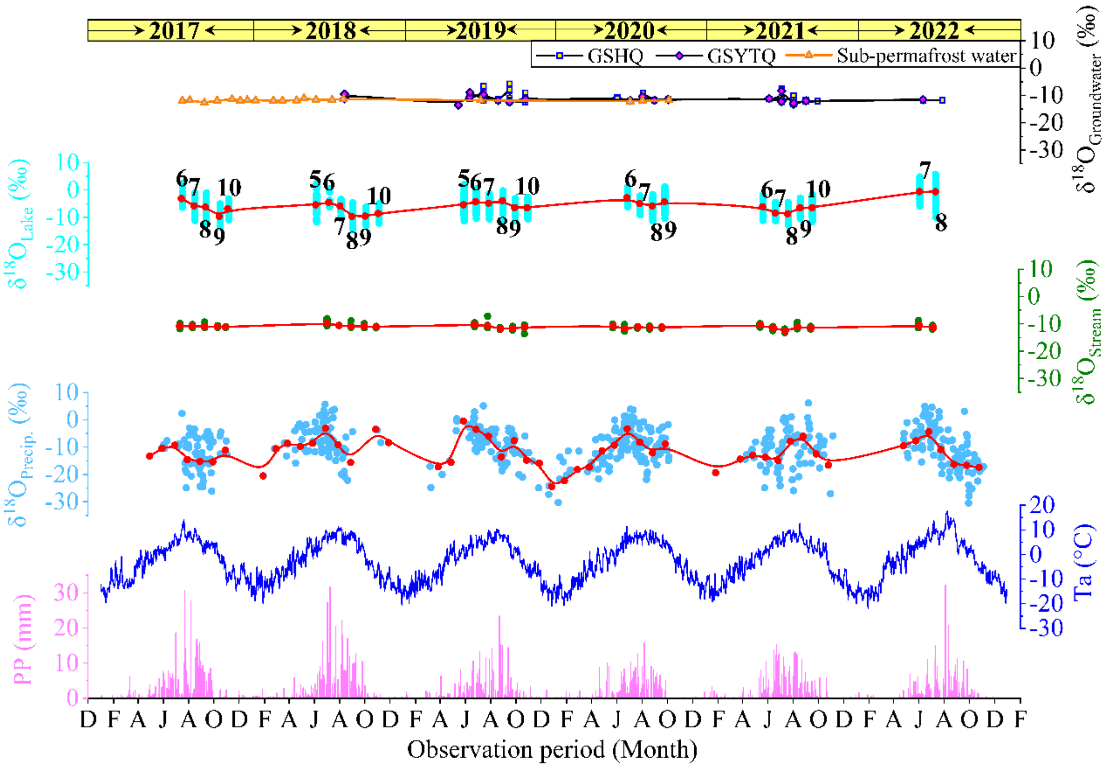

Figure 4: Temporal variations in the $\delta^{18}O$ of different water components in the BLH. The numbers denote the observation months of thermokarst lakes/ponds. The dots with different colours represent event values, while the red dotted line denote the monthly average values. GSHQ and GSYTQ denotes the springs along the both sides of the observation stream and spring in the source area of this stream, respectively.

5.1.3 Ground ice

The distributions of stable isotope dots of all cores are scattered along depths (Fig. 5). Generally, the $\delta^{18}O$ ranging from −15.0‰ to −8.3‰ (mean: -12.2‰), from −113.7‰ to −66.4‰ (mean: -94.4‰) for δD, and between -13.4‰ to 15.5‰ (mean: 3.1‰) for d-excess, respectively. Comparing with the precipitation, majorities of the $\delta^{18}O$ points of ground ice are isotopically lighter than the precipitation, indicating multi-sources of initial water during ice formation under variable climatic conditions and complex geological contexts on the QTP (Michel, 2011; Yang et al., 2017; 2023; Murton, 2013).

Specifically, the stable isotopes of ground ice varied between different boreholes (Fig. 5; Table 4). It is attributed to the influences of initial source water and complex ice formation mechanism. In addition, the isotopic patterns along depths showed marked differences between boreholes (Fig. 5), suggesting influence of lithology on the water migration and freezing fractionation of stable isotopes (Yang et al., 2020; Lacelle, 2014; Fisher et al., 2021). Remarkably, the thaw slump ice was isotopically lighter than those of drilling ground ice (Fig. 5; Table 4), it is due to the considerable differences in the initial source water and freezing processes. The thaw slump ice is considered to replenished by winter snowmelt water via cracks and freezing quickly (Fritz et al., 2011; Porter et al., 2020). However, the pore ice with isotopically light values in these boreholes is suffered isotope fractionation due to freeze-thaw under climate transitions (Wetterich et al., 2014; Yang et al., 2023).

Table 4 General stable isotope composition of ground ice in the Beiluhe Basin

Borehole name	Stable isotopes of ground ice								
	$\delta^{18}O$/‰			δD/‰			d-excess/‰		
	Max	Min	Mean	Max	Min	Mean	Max	Min	Mean
BLH-L-1	-11.7	-14.0	-13.0	-91.0	-102.5	-96.8	9.9	2.8	7.0
BLH-L-2	-10.5	-14.5	-13.2	-86.2	-110.2	-101.9	10.6	-2.5	3.7
BLH-L-3	-11.39	-15.0	-12.8	-92.7	-113.7	-100.6	11.4	-7.1	1.7
BLH-L-4	-9.1	-14.6	-12.3	-80.4	-108.2	-95.5	13.9	-13.3	3.0
BLH-L-5	-10.2	-14.1	-12.7	-89.0	-108.6	-100.2	8.1	-7.3	1.7
BLH-L-6	-10.1	-13.3	-11.6	-86.9	-105.4	-96.1	4.4	-10.3	-2.9
BLH-R-1	-9.3	-13.1	-11.9	-80.3	-100.6	-90.8	9.3	-6.1	4.4
BLH-R-2	-10.0	-14.3	-12.5	-80.9	-102.8	-93.5	15.5	-0.9	6.7
BLH-R-3	-11.5	-14.0	-12.8	-90.8	-103.0	-97.5	11.5	-1.6	4.9
BLH-R-4	-11.0	-14.0	-12.7	-94.6	-102.3	-98.5	11.5	-8.5	3.0
BLH-R-5	-9.6	-13.9	-12.4	-84.8	-103.3	-96.3	11.0	-7.8	3.0
BLH-R-6	-8.4	-14.2	-11.8	-75.2	-108.3	-93.1	9.2	-9.2	1.6
DZK	-8.3	-12.3	-10.8	-66.4	-91.8	-85.1	8.0	-2.6	1.3
ZK-1	-10.3	-12.2	-11.8	-83.6	-89.8	-88.1	8.4	-0.8	6.3
ZK-2	-9.7	-13.1	-11.8	-78.8	-102.1	-93.6	7.4	-13.4	1.2
ZK-3	-9.2	-13.2	-11.4	-74.3	-103.6	-90.9	11.8	-13.2	0.7
ZK-4	-9.1	-12.9	-10.9	-69.9	-96.4	-84.4	9.7	-9.1	3.0
TSI	-14.3	-14.7	-14.5	-93.2	-96.3	-94.9	21.2	20.2	20.9

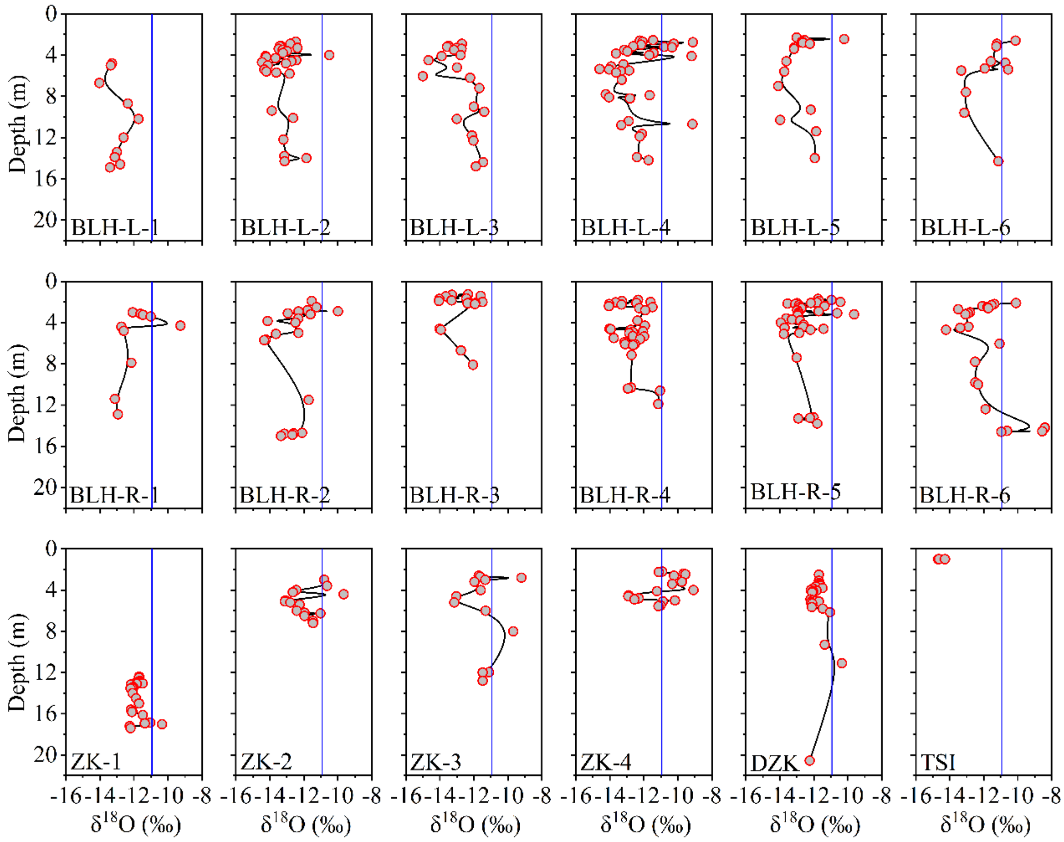

Figure 5: Variations in the stable isotopes of ground ice along depths in the BLH. The blue line denotes the amount-weighted average δ18O value of precipitation in the BLH.

5.2 δ^{18}O-δD relations and hydrological connections

5.2.1 δ^{18}O-δD relationships of different water components

The local meteoric water line (LMWL), determined by three different methods, i.e., ordinary least square regression using the daily isotopic data, the arithmetic mean isotopic values, and the amount-weighted multi-monthly mean isotopic values during six years (2017-2022). They are expressed as: $LMWL_{event}$: $\delta D=7.97\delta^{18}O+15.26$ ($r^2=0.96$), $LMWL_{montyly}$: $\delta D=8.06\delta^{18}O+12.58$ ($r^2=0.93$), $LMWL_{PWA}$: $\delta D=7.78\delta^{18}O+8.78$ ($r^2=0.92$). The slope is nearly identical to that of the global meteoric water line (GMWL; Craig, 1961). However, the intercepts are quietly different (Fig. 6) due to the influences of precipitation amounts and the exceptional meteorological conditions (Barešić et al., 2006; Hughes and Crawford, 2012; Kern et al., 2016).

The δ^{18}O–δD diagrams of lakes, streams, and groundwater were built using the monthly stable isotopic values, and defined as local evaporation line (LELs). The LELs observed during six years are calculated as: $\delta D=5.88\delta^{18}O-12.80$ ($r^2=0.95$), $\delta D=4.89\delta^{18}O-19.41$ ($r^2=0.83$), $\delta D=5.69\delta^{18}O-10.50$

(r^2=0.85) (supra-permafrost water), and δD=3.54δ^{18}O-39.06 (r^2=0.92) (sub-permafrost water), respectively. The slopes of the three LELs are all lower than those of LMWL (Fig. 6), and ranging between 4 and 6, indicating strong evaporation (Cui et al., 2017; Yang et al., 2019) due to lower relative humidity (Clark and Fritz, 1997). Interestingly, the correlation coefficients of streams and supra-permafrost water are much lower (less than 0.9) and the slopes are smaller than those of precipitation and lakes/ponds (Fig. 6), which may be affected by the transitions of source water during warm seasons and the evaporative concentration of isotopes.

The δ^{18}O–δD relationship for ground ice was established using the stable isotopic values of the ice samples, and the correlation is defined as the freezing line (FL; Souchez et al., 2000). In this study, the freezing line of the ground ice at 16 borehole sites were calculated as: δD=5.36δ^{18}O-29.15 (r^2=0.73), which is significantly different from the LMWL (Fig. 6). The difference reflects the freezing characteristics of liquid water under different conditions (Lacelle, 2011). Our freezing slope in between 6.2 and 7.3 were usually obtained during equilibrium freezing Rayleigh-type fractionation (Lacelle, 2011). The lower correlation coefficient (Fig. 6) suggests variable freezing rates (Souchez et al., 2000), kinetic isotopic fractionation during ice formation (Souchez et al., 2000), as well as the influence of the initial source water of the ground ice at different sites (Lacelle, 2011; Yang et al., 2017).

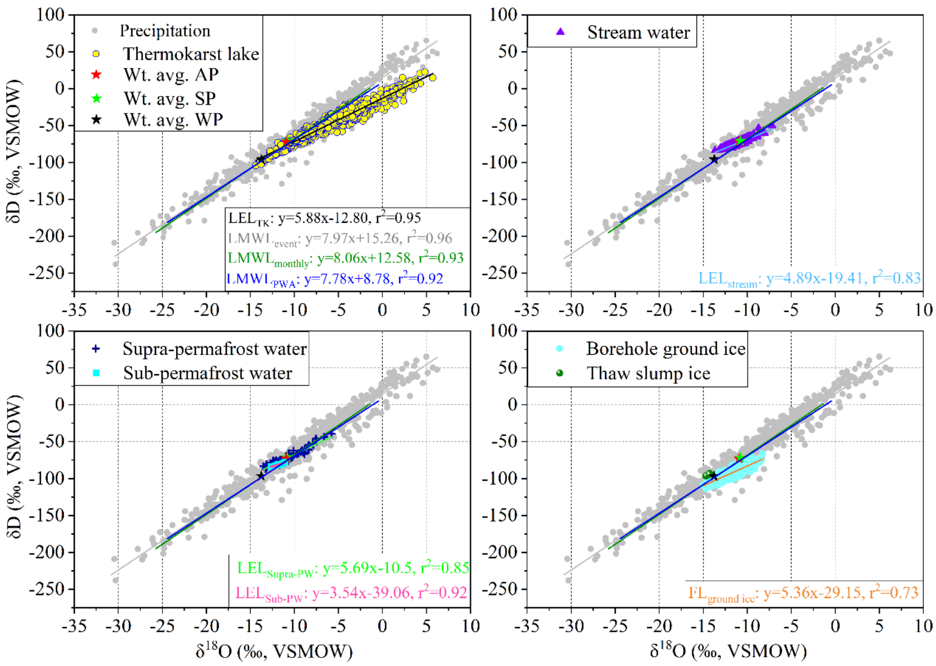

Figure 6: The relation between δD and δ^{18}O of different water components in the BLH. The Wt. avg. SP, Wt. avg. WP, Wt. avg. AP, LEL, and FL denotes the weighted average value of summer precipitation, weighted average value of winter precipitation, weighted average value of annual precipitation, local evaporation line of surface water components, and freezing line of ground ice, respectively.

5.2.2 Hydrological connections between various water components

Majority of the stable isotopes of stream lie on the LMWL (Fig. 6) and embrace in the range of supra-permafrost water (Fig. 7), in addition, the mean value is close to the amount-weighted average value of annual/summer precipitation, indicating the direct recharge of precipitation and supra-permafrost waters. However, partial of the isotopic dots do not lie on the LMWL, exhibit a clear evaporative effect. The supra-permafrost water and sub-permafrost water display concentrated isotopic patterns comparing with precipitation, reflecting relatively stable recharge sources. In addition, the scattered isotopic dots of supra-permafrost water rather than sub-permafrost water indicated changeable sources and climate conditions. For comparison, the partial of isotope points of the supra-permafrost water are overlapping with those of precipitation and stream water, suggesting important replenishment of precipitation and stream. However, the isotopic cluster of sub-permafrost water is significantly deviated from the LMWL and all the isotope values are lower than the annual average value of modern precipitation, suggesting the recharge signal of past water with negative isotopes under cold climate conditions. The LEL of thermokarst lakes/ponds significantly deviated from LMWL (Fig. 6; 7), partial of the isotopic dots overlapped with precipitation, groundwater, and ground ice, indicating the hydrological connections between them (Yang et al., 2016; 2017).

The cluster of ground ice is partly overlapped with precipitation, groundwater, lakes, and stream (Fig. 7). It is indicative of mutual replenishment relations between them. Some of the isotope dots are more positive than the summer precipitation, implying the recharge from evaporative active layer water. A clear freezing slope is shown, indicating typical freezing of liquid water (Jouzel and Souchez, 1982; Souchez and Jouzel, 1984; Lacelle et al., 2011; Perşoiu and Pazdur., 2011). However, the d-excess values of ground ice are lower than those of river water and the amount-weighted average value of annual/summer precipitation (Fig. 7), suggesting the important recharge of active layer water (subjected to evaporation) to the near-surface ground ice (Yang et al., 2013; Throckmorton et al., 2016). In addition, the thaw slump ice exhibited more negative isotopes, which is even lower than the amount-weighted average value of winter precipitation (Fig. 7), indicating the main recharge of snowmelt water (Yang et al., 2020; Opel et al., 2018).

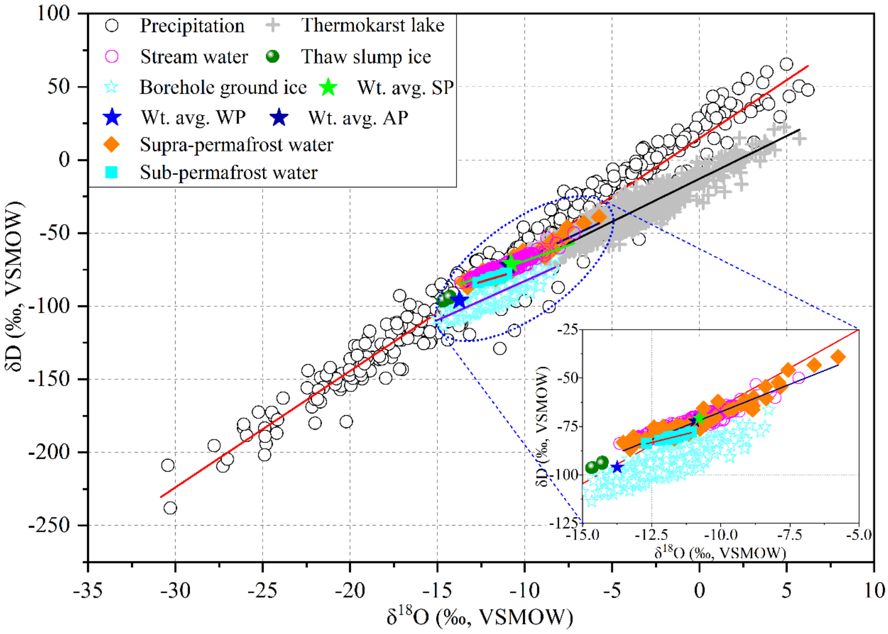

Figure 7: Hydrological connections between different water components.

6 Data availability

The dataset provided in this paper can be obtained at https://doi.org/10.5281/zenodo.10684110 (Yang, 2024). The link will become publicly available until full publication.

7 Conclusions

From 2017 to 2022, we constructed the first stable isotope monitoring network in a typical permafrost-dominated watershed (namely the Beiluhe Basin, BLH) in central Qinghai-Tibet Plateau (QTP). Totally, we obtained 554 precipitation samples, 2402 lakes/ponds samples, 675 stream water samples, 102 supra-permafrost water samples, and 19 sub-permafrost water samples. Importantly, 359 ground ice samples at different depths from 17 boreholes and 2 profiles were collected, which is the first detailed isotopic data of permafrost ice on the QTP. The following findings are drawn:

1) The stable isotopes of precipitation display distinct seasonal patterns with high values in summer and low values in winter. The slope of LMWL is reflected the global mean. However, the intercepts are quietly different due to the influences of precipitation amounts and the exceptional meteorological conditions.

2) The thermokarst lakes/ponds and streams exhibit remarkable seasonal patterns in stable isotopes, which is due to the transition of source waters and evaporation differences. The isotopically

lighter values in August and September are attributed to the recharges of monsoonal precipitation and melting ground ice. Evaporation enrichment and recharges of precipitation with heavier isotopes greatly influenced the isotopic patterns in May, June, July, and October. The slopes of the three LELs are all lower than those of LMWL, indicating strong evaporation due to lower relative humidity. The supra-permafrost water was recharged by precipitation via infiltration. By contrast, the sub-permafrost water was replenished by unchanged sources of isotopically lighter water during cold periods.

3) The stable isotopes of ground ice varied between different boreholes. It is attributed to the influences of initial source water and complex ice formation mechanism. The near-surface ground ice was closely related to the recent precipitation and active layer hydrology, however, the deep-layer ground ice exhibited complicated formation mechanism. In addition, variability in the isotopic patterns along depths suggested influence of lithology on the water migration and freezing fractionation of stable isotopes. The freezing line of the ground ice is significantly different from the LMWL, reflected the freezing characteristics of liquid water under different conditions.

This first comprehensive data set provides a new basis for studying the isotopic hydrology and exploring the hydrological effects of degrading permafrost on the QTP. It also enriches the cryospheric database of the Northern Hemisphere.

Author contributions

YY and QW conceived the idea of the study. YY designed the isotope observation network and completed the manuscript. XG and ZZ analyzed water samples and plotted figures. LZ, HY, and DZ participated the field work. JC and GL provided and analyzed the meteorological data.

Acknowledgements

This work was supported by the Key Research Program of Frontier Sciences, CAS (Grant No. ZDBS–LY–DQC026), the National Natural Science Foundation of China (Grant No. 41871062; 42177073), and the foundation of the State Key Laboratory of Frozen Soil Engineering (Grant No. SKLFSE–ZT–202118). We give special thanks to Hongtan, Yandong Hou, Jing Zhan, Siru Gao, Guanli Jiang, and Peng Zhang for their kind help during field sampling work.

References

[1] Aichner, B., Dubbert, D., Kiel, C., Kohnert, K., Ogashawara, I., Jechow, A., ... & Berger, S. A. 2022. Spatial and seasonal patterns of water isotopes in northeastern German lakes. Earth System Science Data, 14(4), 1857-1867.

[2] Ala-aho, P., Soulsby, C., Pokrovsky, O., Kirpotin, S.N., Karlsson, J.P., Serikova, S., Manasypov, R., Lim, A., Krickov, I., Kolesnichenko, L.G., 2018. Permafrost and lakes control river isotope composition across a boreal-arctic transect in the Western Siberia lowlands. Environmental Research Letters, 13(3): 034028.

[3] Barešić, J., Horvatinčić, N., Krajcar Bronić, I., Obelić, B., & Vreča, P. 2006. Stable isotope composition of daily and monthly precipitation in Zagreb. Isotopes in Environmental and Health Studies, 42(3), 239-249.

[4] Bershaw, J.; Penny, S.M.; Garzione, C.N. 2012. Stable isotopes of modern water across the Himalaya and eastern Tibetan Plateau: Implications for estimates of paleoelevation and paleoclimate. J. Geophys. Res. Atmos, 117.

[5] Biskaborn, B.K., Smith, S.L., Noetzli, J., Matthes, H., Vieira, G., Streletskiy, D.A., ... & Lantuit, H., 2019. Permafrost is warming at a global scale. Nature Communications, 10(1), 264.

[6] Brown, J., Sidlauskas, F. J., & Delinski, G. F. 1997. (Eds.): Circum-Arctic map of permafrost and ground ice conditions. Washington, DC: U.S. Geological Survey in Cooperation with the Circum-Pacific Council for Energy and Mineral Resources, Circum-Pacific Map Series CP-45, scale 1:10,000,000, 1 sheet.

[7] Cheng, G., Zhao, L., Li, R., Wu, X., Sheng, Y., Hu, G., Zou, D., Jin, H., Li, X., Wu, Q., 2019. Characteristic, changes and impacts of permafrost on Qinghai-Tibet Plateau. Chinese Science Bulletin, 64(27), 2783-2795.

[8] Cheng, G.D., Jin, H.J. 2013. Permafrost and Groundwater on the Qinghai-Tibet Plateau and in Northeast China. Hydrogeology Journal, 21 (1): 5-23.

[9] Clark, I., Fritz, P. 1997. Environmental Isotopes in Hydrogeology. Lewis Publishers, Boca Raton – New York.

[10] Connon RF, Quinton WL, Craig JR, Hayashi M. 2014. Changing hydrologic connectivity due to permafrost thaw in the lower Liard River valley, NWT, Canada. Hydrological Processes, 28(14): 4163–4178.

[11] Craig, H. 1961. Isotopic variations in meteoric waters. Science, 133(3465), 1702-1703.

[12] Cui, J., Tian, L., Biggs, T. W., & Wen, R. 2017. Deuterium-excess determination of evaporation to inflow ratios of an alpine lake: Implications for water balance and modeling. Hydrological Processes, 31(5), 1034-1046.

[13] Douglas, T. A., Hiemstra, C. A., Anderson, J. E., Barbato, R. A., Bjella, K. L., Deeb, E. J., ... & Wagner, A. M., 2021. Recent degradation of Interior Alaska permafrost mapped with ground surveys, geophysics, deep drilling, and repeat airborne lidar. The Cryosphere, 15(8), 3555-3575.

[14] Fisher, D.A., Lacelle, D., Pollard, W., Faucher, B., 2021. A model for stable isotopes of residual liquid water and ground ice in permafrost soils using arbitrary water chemistries and soil-specific empirical residual water functions. Permafrost and Periglacial Processes, 32(2): 248-260.

[15] Fritz, M., Wetterich, S., Meyer, H., Schirrmeister, L., Lantuit, H., & Pollard, W. H. 2011. Origin and characteristics of massive ground ice on Herschel Island (western Canadian Arctic) as revealed by stable water isotope and hydrochemical signatures. Permafrost and Periglacial Processes, 22(1), 26-38.

[16] Gibson, J. J., Birks, S. J., Yi, Y., & Vitt, D. 2015. Runoff to boreal lakes linked to land cover, watershed morphology and permafrost thaw: a 9-year isotope mass balance assessment. Hydrological Processes, 29(18), 3848-3861.

[17] Guan, H., Zhang, X., Skrzypek, G., Sun, Z. and Xu, X., 2013. Deuterium excess variations of rainfall events in a coastal area of South Australia and its relationship with synoptic weather systems and atmospheric moisture sources. Journal of Geophysical Research: Atmospheres, 118(2), 1123–1138.

[18] Guo, D., Wang, H., Wang, A., 2017. Sensitivity of historical simulation of the permafrost to different atmospheric forcing data sets from 1979 to 2009. Journal of Geophysical Research: Atmospheres, 122(22), 12-269.

[19] Guo, X., Feng, Q., Si, J., & Zhang, X. 2022. Considerable influences of recycled moistures and summer monsoons to local precipitation on the northeastern Tibetan Plateau. Journal of Hydrology, 605, 127343.

[20] Hughes, C. E., & Crawford, J. 2012. A new precipitation weighted method for determining the meteoric water line for hydrological applications demonstrated using Australian and global GNIP data. Journal of Hydrology, 464, 344-351.

[21] Immerzeel, W. W., Van Beek, L. P., & Bierkens, M. F. 2010. Climate change will affect the Asian water towers.

Science, 328(5984), 1382-1385.

[22] IPCC, 2019: Climate Change and Land: an IPCC special report on climate change, desertification, land degradation, sustainable land management, food security, and greenhouse gas fluxes in terrestrial ecosystems.

[23] Jouzel, J., Souchez, R. A. 1982. Melting–refreezing at the glacier sole and the isotopic composition of the ice. Journal of Glaciology, 28(98), 35-42.

[24] Kern, Z., Harmon, R. S., & Fórizs, I. 2016. Stable isotope signatures of seasonal precipitation on the Pacific coast of central Panama. Isotopes in Environmental and Health Studies, 52(1-2), 128-140.

[25] Knapp, J.L., Neal, C., Schlumpf, A., Neal, M., Kirchner, J.W., 2019. New water fractions and transit time distributions at Plynlimon, Wales, estimated from stable water isotopes in precipitation and streamflow. Hydrology and Earth System Sciences, 23(10): 4367-4388.

[26] Kuang, X., & Jiao, J. J. 2016. Review on climate change on the Tibetan Plateau during the last half century. Journal of Geophysical Research: Atmospheres, 121(8), 3979-4007.

[27] Lacelle, D. 2011. On the $\delta^{18}O$, δD and D-excess relations in meteoric precipitation and during equilibrium freezing: theoretical approach and field examples. Permafrost and Periglacial Processes, 22(1), 13-25.

[28] Lacelle, D., Fontaine, M., Forest, A. P., & Kokelj, S. 2014. High-resolution stable water isotopes as tracers of thaw unconformities in permafrost: A case study from western Arctic Canada. Chemical Geology, 368, 85-96.

[29] Lacelle, D., Vasil'chuk, Y. K., 2013. Recent progress (2007–2012) in permafrost isotope geochemistry. Permafrost and Periglacial Processes, 24(2), 138-145.

[30] Lawrence, D. M., Slater, A. G., 2005. A projection of severe near-surface permafrost degradation during the 21st century. Geophysical Research Letters, 32(24).

[31] Liu, F., Qin, S., Fang, K., Chen, L., Peng, Y., Smith, P., & Yang, Y. 2022a. Divergent changes in particulate and mineral-associated organic carbon upon permafrost thaw. Nature Communications, 13(1), 5073.

[32] Liu, L., Zhuang, Q., Zhao, D., Zheng, D., Kou, D., & Yang, Y. 2022b. Permafrost Degradation Diminishes Terrestrial Ecosystem Carbon Sequestration Capacity on the Qinghai-Tibetan Plateau. Global Biogeochemical Cycles, 36(2), e2021GB007068.

[33] Luo, J., Niu, F., Lin, Z., Liu, M., & Yin, G. 2015. Thermokarst lake changes between 1969 and 2010 in the Beilu River basin, Qinghai–Tibet plateau, China. Science Bulletin, 60(5), 556-564.

[34] Michel, F. A., 2011. Isotope characterisation of ground ice in northern Canada. Permafrost and Periglacial Processes, 22(1), 3-12.

[35] Murton, J.B., 2013. Ground Ice and Cryostratigraphy. In: Shroder, J.F. (Ed.), Treatise on Geomorphology. Academic Press, San Diego. 173-201.

[36] Narancic, B., Wolfe, B.B., Pienitz, R., Meyer, H., Lamhonwah, D., 2017. Landscape-gradient assessment of thermokarst lake hydrology using water isotope tracers. Journal of Hydrology, 545: 327-338.

[37] Niu, F., Lin, Z., Liu, H., & Lu, J. 2011. Characteristics of thermokarst lakes and their influence on permafrost in Qinghai–Tibet Plateau. Geomorphology, 132(3-4), 222-233.

[38] Opel, T., Meyer, H., Wetterich, S., Laepple, T., Dereviagin, A., Murton, J., 2018. Ice wedges as archives of winter paleoclimate: A review. Permafrost and Periglacial Processes, 29(3): 199-209.

[39] Perşoiu, A., & Pazdur, A. 2011. Ice genesis and its long-term mass balance and dynamics in Scărişoara Ice Cave, Romania. The Cryosphere, 5(1), 45-53.

[40] Porter, T. J., & Opel, T. 2020. Recent advances in paleoclimatological studies of Arctic wedge-and pore-ice stable-water isotope records. Permafrost and Periglacial Processes, 31(3), 429-441.

[41] Porter, T.J., Schoenemann, S.W., Davies, L.J., Steig, E.J., Bandara, S., Froese, D.G., 2019. Recent summer warming in northwestern Canada exceeds the Holocene thermal maximum. Nature Communications, 10(1): 1631.

[42] Quinton WL, Baltzer LJ. 2013. The active-layer hydrology of a peat plateau with thawing permafrost (scotty creek, canada). Hydrogeology Journal, 21 (1): 201-220.

[43] Ran, Y., Li, X., Cheng, G., Che, J., Aalto, J., Karjalainen, O., ... & Chang, X. 2022. New high-resolution estimates of the permafrost thermal state and hydrothermal conditions over the Northern Hemisphere. Earth System Science Data Discussions, 14 (2), 865–884.

[44] Rogger M, Chirico G, Hausmann H, Krainer K, Brückl E, Stadler P, Blöschl G. 2017. Impact of mountain permafrost

on flow path and runoff response in a high alpine catchment. Water Resources Research, 53(2):1288-1308.
[45] Schwamborn G, Meyer H, chirrmeister L, G, F., 2014. Past freeze and thaw cycling in the margin of the El'gygytgyn Crater deduced from a 141m long permafrost record. Climate of the Past, 10: 1109-1123.
[46] Song, C., Wang, G., Liu, G., Mao, T., Sun, X., & Chen, X. (2017). Stable isotope variations of precipitation and streamflow reveal the young water fraction of a permafrost watershed. Hydrological Processes, 31(4), 935-947.
[47] Souchez, R. A., & Jouzel, J. 1984. On the isotopic composition in δD and $\delta^{18}O$ of water and ice during freezing. Journal of Glaciology, 30(106), 369-372.
[48] Souchez, R., Jouzel, J., Lorrain, R., Sleewaegen, S., Stiévenard, M., & Verbeke, V. 2000. A kinetic isotope effect during ice formation by water freezing. Geophysical Research Letters, 27(13), 1923-1926.
[49] Streletskiy, D.A., Tananaev, N.I., Opel, T., Shiklomanov, N.I., Nyland, K.E., Streletskaya, I.D., Shiklomanov, A.I., 2015. Permafrost hydrology in changing climatic conditions: seasonal variability of stable isotope composition in rivers in discontinuous permafrost. Environmental Research Letters, 10(9): 095003.
[50] Throckmorton, H. M., Newman, B. D., Heikoop, J. M., Perkins, G. B., Feng, X., Graham, D. E., ... & Wilson, C. J. 2016. Active layer hydrology in an arctic tundra ecosystem: quantifying water sources and cycling using water stable isotopes. Hydrological Processes, 30(26), 4972-4986.
[51] Tian, L., Yao, T., White, J.W.C., Yu, W., Wang, N., 2005. Westerlies moisture transport to the middle of Himalayas revealed from the high deuterium excess. Chinese Science Bulletin, 50(10), 1026–1030.
[52] Vasil'chuk, Y.K., Lawson, D.E., Yoshikawa, K., Budantseva, N.A., Chizhova, J.N., Podborny, Y.Y., Vasil'chuk, A.C., 2016. Stable isotopes in the closed-system Weather Pingo, Alaska and Pestsovoye Pingo, northwestern Siberia. Cold Regions Science and Technology, 128: 13-21.
[53] Vystavna, Y., Harjung, A., Monteiro, L. R., Matiatos, I., & Wassenaar, L. I. 2021. Stable isotopes in global lakes integrate catchment and climatic controls on evaporation. Nature Communications, 12(1), 7224.
[54] Wang, G., Li, Y., Wu, Q., & Wang, Y. 2006. Impacts of permafrost changes on alpine ecosystem in Qinghai-Tibet Plateau. Science in China Series D: Earth Sciences, 49, 1156-1169.
[55] Wang, S., He, X., Kang, S., Fu, H., & Hong, X. 2022. Estimation of stream water components and residence time in a permafrost catchment in the central Tibetan Plateau using long-term water stable isotopic data. The Cryosphere, 16(12), 5023-5040.
[56] Wang, S., He, X., Kang, S., Hong, X., Fu, H., Xue, Y., ... & Guo, H. 2023b. Assessment of streamwater age using water stable isotopes in a headwater catchment of the central Tibetan Plateau. Journal of Hydrology, 618, 129175.
[57] Wang, T., Yang, D., Yang, Y., Zheng, G., Jin, H., Li, X., ... & Cheng, G. 2023a. Unsustainable water supply from thawing permafrost on the Tibetan Plateau in a changing climate. Science Bulletin, S2095-9273.
[58] Wetterich, S., Tumskoy, V., Rudaya, N., Andreev, A. A., Opel, T., Meyer, H., ... & Hüls, M. 2014. Ice Complex formation in arctic East Siberia during the MIS3 Interstadial. Quaternary Science Reviews, 84, 39-55.
[59] Wu, Q., & Zhang, T. 2010. Changes in active layer thickness over the Qinghai-Tibetan Plateau from 1995 to 2007. Journal of Geophysical Research: Atmospheres, 115(D9).
[60] Yang, K., Ye, B., Zhou, D., Wu, B., Foken, T., Qin, J., & Zhou, Z. 2011. Response of hydrological cycle to recent climate changes in the Tibetan Plateau. Climatic Bhange, 109, 517-534.
[61] Yang, Y., Guo, X., Wu, Q., Jin, H., & Liu, F. 2023. Formation processes of shallow ground ice in permafrost in the Northeastern Qinghai-Tibet Plateau: A stable isotope perspective. Science of The Total Environment, 863, 160967.
[62] Yang, Y., Wu, Q., Jiang, G., Zhang, P., 2017. Stable Isotopic Stratification and Growth Patterns of Ground Ice in Permafrost on the Qinghai-Tibet Plateau, China. Permafrost and Periglacial Processes, 28(1), 119-129.
[63] Yang, Y., Wu, Q., Jiang, G., Zhang, P., 2020. Ground ice at depths in the Tianshuihai Lake basin on the western Qinghai-Tibet Plateau: An indication of permafrost evolution. Science of the Total Environment,729, 138966.
[64] Yang, Y., Wu, Q., Jin, H., Wang, Q., Huang, Y., Luo, D., Gao, S., Jin, X., 2019. Delineating the hydrological processes and hydraulic connectivities under permafrost degradation on Northeastern Qinghai-Tibet Plateau, China. Journal of hydrology, 569, 359-372.
[65] Yang, Y., Wu, Q., Liu, F., & Jin, H. 2021. Spatial-temporal trends of hydrological transitions in thermokarst lakes on Northeast Qinghai-Tibet Plateau based on stable isotopes. Journal of Hydrology, 597, 126314.
[66] Yang, Y., Wu, Q., Yun, H., 2013. Stable isotope variations in the ground ice of Beiluhe Basin on the Qinghai-Tibet

Plateau. Quaternary International, 313, 85-91.
[67] Yang, Y., Wu, Q., Yun, H., Jin, H., Zhang, Z., 2016. Evaluation of the hydrological contributions of permafrost to the thermokarst lakes on the Qinghai–Tibet Plateau using stable isotopes. Global and Planetary Change, 140, 1-8.
[68] Yao, T., Masson-Delmotte, V., Gao, J., Yu, W., Yang, X., Risi, C., Sturm, C., Zhao, H., He, Y. and Ren, W., 2013. A review of climatic controls on $\delta^{18}O$ in precipitation over the Tibetan Plateau: Observations and simulations. Reviews of Geophysics, 51(4), 525–548.
[69] Yao, T., Qin, D., Shen, Y., Zhao, L., Wang, N., Lu, A., 2013. Cryospheric changes and their impacts on regional water cycle and ecological conditions in the Qinghai-Tibetan Plateau. Chin. J. Nat, 35(3), 179-186.
[70] Yi, S., Wang, X., Qin, Y., Xiang, B., & Ding, Y. 2014. Responses of alpine grassland on Qinghai–Tibetan plateau to climate warming and permafrost degradation: a modeling perspective. Environmental Research Letters, 9(7), 074014.
[71] Yin, G., Niu, F., Lin, Z., Luo, J., & Liu, M. 2017. Effects of local factors and climate on permafrost conditions and distribution in Beiluhe basin, Qinghai-Tibet Plateau, China. Science of the Total Environment, 581, 472-485.
[72] Zhang X, He J, Zhang J, Polyakov I, Gerdes R, Inoue J, Wu P. 2013. Enhanced poleward moisture transport and amplified northern high-latitude wetting trend. Nature Climate Change, 3: 47-51.
[73] Zhang, T., Frauenfeld, O.W., Serreze, M.C., Etringer, A., Oelke, C., McCreight, J., Barry, R.G., Gilichinsky, D., Yang, D., Ye, H., Ling, F., Chudinova, S., 2005. Spatial and temporal variability in active layer thickness over the Russian Arctic drainage basin. Journal of Geophysical Research: Atmospheres, 110(D16), 1-14.
[74] Zhao, L., Zou, D., Hu, G., Du, E., Pang, Q., Xiao, Y., Li, R., Sheng, Y., Wu, X., Sun, Z., Wang, L., Wang, C., Ma, L., Zhou, H., Liu, S., 2020. Changing climate and the permafrost environment on the Qinghai–Tibet (Xizang) Plateau. Permafrost and Periglacial Processes, 31(3), 396-405.
[75] Zhao, L., Zou, D., Hu, G., Wu, T., Du, E., Liu, G., ... & Cheng, G. 2021. A synthesis dataset of permafrost thermal state for the Qinghai–Tibet (Xizang) Plateau, China. Earth System Science Data, 13(8), 4207-4218.
[76] Zhu, G., Liu, Y., Shi, P., Jia, W., Zhou, J., Liu, Y., ... & Zhao, K. 2022. Stable water isotope monitoring network of different water bodies in Shiyang River basin, a typical arid river in China. Earth System Science Data, 14(8), 3773-3789.